IEEE Access
Multidisciplinary | Rapid Review | Open Access Journal

Received October 24, 2021, accepted November 28, 2021, date of publication December 15, 2021, date of current version January 21, 2022.

Digital Object Identifier 10.1109/ACCESS.2021.3135926

A Lens-Array-Based Measurement Technique for Spatial Angle

CUNLIANG CAI[1,2], YUFENG YAN[1,2], LEI ZHANG[3], MINGXIN DU[1], AND XIN YU[1,2]

[1]National Demonstration Center for Experimental Optoelectronic Engineering Education, School of Optoelectronic Engineering, Changchun University of Science and Technology, Changchun 130022, China
[2]Key Laboratory of Optoelectronic Measurement and Optical Information Transmission Technology of Ministry of Education, School of Optoelectronic Engineering, Changchun University of Science and Technology, Changchun 130022, China
[3]Unit 63867, PLA, Beijing 100832, China

Corresponding author: Yufeng Yan (yanyufeng_cust@126.com)

This work was supported in part by the Jilin Science and Technology Department, China, under Grant 20210201139GX; in part by the 111 Project of China under Grant D21009; and in part by the National Demonstration Center for Experimental Opto-Electronic Engineering Education.

ABSTRACT Accurate measurement of the spatial angle is key for plane flatness and guide rail straightness detection. This paper presents a lens-array-based optical system and an analytical model for micro-spatial angle measurements. In this system, a collimated light beam passes through four-array lenses arranged in a pyramid shape and forms regular array spots on a charge-coupled device sensor. The angles with respect to the X and Y axes are calculated by analyzing the distance of these spots on the CCD, the distance between adjacent apertures on the lens array, and the inclination angle between the lens array and the CCD. Using the coordinate value of the array spots on the CCD, the angle around the *Z-axis* can also be calculated simultaneously. Finally, the accuracy of the proposed method was verified by comparing the measured results with those of the autocollimator, and it was shown that the proposed approach enabled the achievement of RMS $\leq 0.1''$. Additionally, this measurement system which is consists of a laser source, lens arrays and CCD, compared with other methods, is smaller in volume and more convenient to carry.

INDEX TERMS Image edge detection, measurement by laser beam, optical arrays.

I. INTRODUCTION

In the aerospace field, owing to the influence of gravity, solar radiation, mechanical vibration, and other factors, the connecting arm between the payload and datum point is slightly deformed during the flight of the spacecraft [4], [5]. The payload deflects at a small angle from the datum, which affects its performance. If the deflection of a small angle can be measured in real time and accurately, the influence can be reduced or even eliminated by software compensation, which requires the measurement system to have the characteristics of a small volume, low power consumption and high precision. In addition, in deep-space laser communication, it is necessary to maintain the accurate alignment and tracking of two communication terminals, which is the key to the successful establishment and maintenance of optical communication links, and the angle measurement is also a guarantee of optical communication systems. Therefore, angle measurement systems with small volumes, low power consumption and high precision will have wide application prospects in aerospace, aviation and national defense technologies.

At present, methods for detecting small angles are mainly based on the theory of optical angle measurement, such as the autocollimation method [6]–[9], grating method [10], Fresnel double prism method [11], laser interferometry [12], and image processing [13], [14]. The autocollimation method can use the position of the reflected image points to realize angle measurement, and its measurement accuracy is determined by the distance between the optical elements. Konyakhin *et al.* eliminated the influence of the vignetting error through a compensation algorithm and improved the measurement accuracy of the autocollimator [15]. This method can satisfy the measurement of the dimensional angle. The diffraction grating can also be used as a receiving device for the laser autocollimator. However, because the angular distance between the incident beam and the axis of the autocollimator unit is an unknown parameter, laser autocollimators with diffraction gratings can only be used to measure relative angles. In this method [16], the femtosecond laser and diffraction grating are used as the measurement source and reflector,

The associate editor coordinating the review of this manuscript and approving it for publication was Shuihua Wang.

respectively, and the one-dimensional angular displacement can be accurately identified using the light emitted by the reflector and the first-order diffraction beam of the femtosecond optical comb. A Fresnel double prism was used to create a compound interferometer. Under the background of a double-beam interference fringe, four beam interference patterns can be obtained, and then the angle measurement or calibration can be realized by changing the relative axial position of the double prism relative to the shear direction. However, the measurement system of a Fresnel prism is relatively complex, which limits the application of this method. These methods usually have the advantages of high sensitivity and precision, but their optical system is relatively complex, the system volume is large, the environmental adaptability is relatively poor, and they generally can only measure the relative angle of pitch or azimuth.

In many engineering applications, angle measurement still has some key technologies that need to be studied further, such as real-time measurement, high precision, and miniaturization. The optical method an effective way to solve the problem of angle measurements. In this paper, a micro-spatial angle measurement optical system based on a lens array is proposed. The system mainly consists of a laser source, lens array, and CCD. Using this method, the three angles of pitch, azimuth (yaw), and roll can be obtained simultaneously. To perform the measurement, the collimating beam passed through a pyramid of four arrays of lenses that served as emits, and the CCD formed an array of spots that served as receivers. Then the digital image is processed to obtain the pitch and yaw angles of the transmitting end to the receiving end lattice, and the roll angle of the incident beam can be determined by the rotation of the lattice on the CCD. Finally, the position angle in three-dimensional space can be obtained. The measuring system presented in this study is portable and has a smaller volume.

II. MEASUREMENT PRINCIPLE

In the measurement, the incident angle between the laser collimating beam and the receiving surface of the CCD was measured by combining the lens array with the CCD camera. As shown in Fig. 1, the lens arrays are positioned in front of the CCD receiver in a pyramidal arrangement. When the focal plane of the array lens was at a certain angle to the receiving surface of the CCD, the distance between the array spots varied with the angle of the incident beam. Therefore, the mathematical relationship between the array spot distance and the angle of the incident beam can be established to measure the small angle. In this measurement method, two more system parameters are introduced than in the traditional measurement method, that is, the inclination angle between the focal plane of the array lens and the CCD receiving plane and the lens distance. This measuring system can be widely used in the engineering application of angle measurements.

As shown in Fig. 1(a), four lens arrays labeled 1 to 4 for measuring the angle information in three-dimensional space are symmetrically distributed in the horizontal and vertical

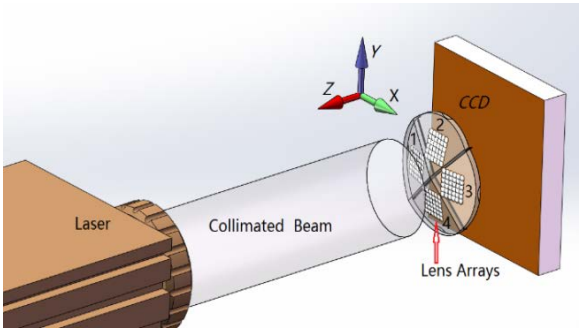

(a) Schematic diagram of the system principle and structure

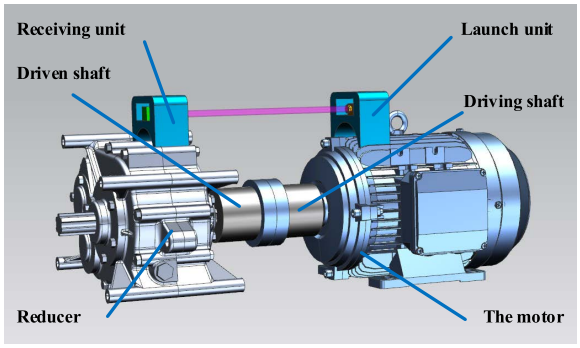

(b) Schematic diagram of the system application and structure

FIGURE 1. Schematic diagram of the system structure.

directions. Lens arrays 1 and 3 were distributed in the horizontal direction and the rest were distributed in the vertical direction. The angle between each lens array and the CCD receiving surface was equal, and the angle between the focal plane and the CCD surface was equal. Lens arrays 1 and 3 in the horizontal direction were used to measure the component of the incident angle in the *X-direction*, and lens arrays 2 and 4 in the vertical direction were used to measure the component of the incident angle in the *Y-direction*.

As shown in Fig. 1(b), the application scenario is the detection of deviations in axis pairs. The transmitting unit of the angle-measuring device was installed on the motor connected to the driving shaft at the right end, and the receiving unit was installed on the reducer connected to the driven shaft at the left end. The pitch angle, azimuth angle and roll angle of the reducer relative to the motor are obtained by measuring the incident angle between the laser collimating beam from the transmitter and the CCD receiving surface of the receiver, and by reference conversion.

III. THE ANALYTICAL MODELING

The mathematical analytic relation of the incident inclination in the *X-direction* is consistent with that in the *Y-direction*. In this section, we describe only the establishment process in the *Y-direction* and around the *Z-axis*.

A. FOR THE PITCH AND YAW ANGLES

As shown in Fig. 2, when the incident beam is only tilted in the *Y-direction* (rotated about the *Z-axis*), the centers of the two lens arrays are represented by O_1 and O_2, and the normal lines of the CCD receiving surface are represented by O_1A_1

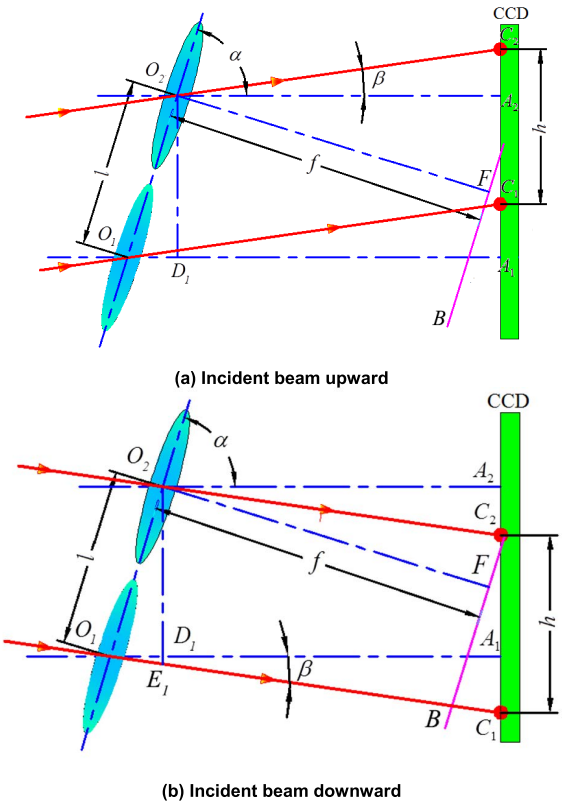

FIGURE 2. Schematic diagram of the incident beam.

and O_2A_2. β is the inclined angle of the measured beam, that is, the included angle between the optical axis of the incident beam and the normal of the CCD receiving surface. C_1 and C_2 represent the positions of the centroid of the spot on the CCD. FB is the focal plane of the lens array and O_2F is perpendicular to FB, where F is the intersection point. For the other parameters shown in Fig. 2, f is the focal length of the lens array, l is the distance between the lenses in the lens array, α is the relative angle between the lens array and CCD, and h is the distance between the center of mass of the adjacent spots.

According to the geometric relationship shown in Fig. 2(a), the incident angle β of the measured beam can be calculated using (1):

$$\tan\beta = \frac{l\sin\alpha - h}{l\cos\alpha} \tag{1}$$

Then, the incident angle β_y of the beam in the *Y-direction* can be expressed using (2):

$$\beta_y = \arctan\frac{l\sin\alpha - h_y}{l\cos\alpha} \tag{2}$$

A schematic diagram of the downward case is shown in Fig. 2(b). By extending O_2D_1 and O_1C_1 to point E_1, the angle β_y for the incident beam can be calculated using (3):

$$\beta_y = -\arctan\frac{l\sin\alpha - h_y}{l\cos\alpha} \tag{3}$$

The results show that only the positive and negative values are different when calculating the incident angles of the

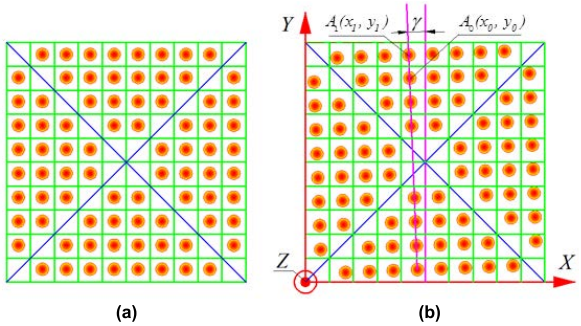

FIGURE 3. Schematic diagram for the roll angle: (a) The spots schematic diagram when the roll angle is 0, (b) The spots schematic diagram when the roll angle is γ.

measured beam in different directions. The positive and negative signs in both the equations indicate the incident direction of the measured beam.

Therefore, the angle β_y of the incident beam in the oblique *Y-direction* can also be calculated using (4):

$$\beta_y = \pm\arctan\frac{l\sin\alpha - h_y}{l\cos\alpha} \tag{4}$$

B. FOR THE ROLL ANGLE

The roll angle is the tilt angle around the *Z-axis*, which is the angle of the beam base plane relative to the CCD base plane. Ideally, when the roll angle is 0°, the schematic diagram of the spot array received by the CCD is shown in Fig. 3(a). The centroid coordinates of the spot array in the same column or row are the same, and the position of the center of the spot can be regarded as the reference position.

When a roll angle occurs, the coordinates of the array spot are offset, as shown in Fig. 3(b). Thus, the roll angle can be calculated from the centroid offset of the spot. The roll angle is expressed as (5),

$$\gamma = \arctan(\frac{x_0 - x_1}{y_0 - y_1}) \tag{5}$$

where (x_0, y_0) and (x_1, y_1) are the centroid coordinates of spots A_0 and A_1, respectively.

Multiple groups of roll angle data can be obtained by changing the coordinates of multiple array spots. To reduce the random error, the average value of the roll angle is introduced, and the systematic error caused by manufacturing and assembly can be obtained through the calculation of multiple array spots.

C. FOR THE ANGLE α

To measure the beam incidence angle, it can be determined from (2) and (3) that the beam incidence angle is related to the center distance between adjacent lens elements in the lens array, spot distance, and relative angle between the lens array and CCD receiving surface. The center distance between adjacent lens elements in the lens array is a fixed value that can be calculated and the spot distance can be obtained through image processing; the angle α (the relative angle between the lens array and the CCD receiving surface)

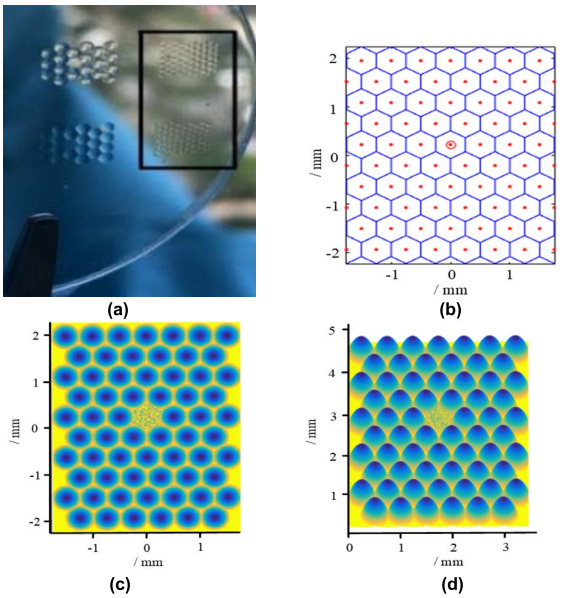

FIGURE 4. Physical picture and simulation charts of array lens: (a) Physical picture of array lens, (b) Size picture of array lens, (c) Top view of array lens, (d) Side view of array lens.

belongs to the installation parameter. The value of α must be calibrated during the first measurement. To ensure the accuracy of the measurement system, the optimal compensation value of α can be obtained through data fitting of the relevant experimental data.

As can be seen from (2) and (3), when the beam incident angle β is unknown and the spot distance h is known, the value of α cannot be calculated using a single variable h. Therefore, multiple groups of data can be used to calculate α together and compensate. (2) can be expressed as (6):

$$h = l\sin\alpha - l\cos\alpha\tan\beta \tag{6}$$

In (6), given the unknown quantity β a small increment $\Delta\beta$ in turn, the initial unknown quantity β is represented by β_0, and H changes with the increment $\Delta\beta$, so we can obtain (7):

$$\begin{cases} h_1 = l\sin\alpha - l\cos\alpha\tan(\beta_0 + \Delta\beta_1) \\ h_2 = l\sin\alpha - l\cos\alpha\tan(\beta_0 + \Delta\beta_2) \\ \vdots \\ h_n = l\sin\alpha - l\cos\alpha\tan(\beta_0 + \Delta\beta_n) \end{cases} \tag{7}$$

where l is a known quantity, α and β_0 are unknown quantities, and h changes with increment $\Delta\beta$. Therefore, $\Delta\beta_i (1 \leqslant i \leqslant n)$ can be regarded as the independent variable and $h_i (1 \leqslant i \leqslant n)$ as the dependent variable, that is,

$$h_i = l\sin\alpha - l\cos\alpha\tan(\beta_0 + \Delta\beta_i) \tag{8}$$

Equation (8) passes through points $(\Delta\beta_1, h_1)$, $(\Delta\beta_2, h_2), \ldots, (\Delta\beta_n, h_n)$, where α and β_0 are unknown parameters. Parameter α was obtained and compensated by means of curve fitting.

IV. PARAMETER ANALYSIS OF LENS ARRAY

In order to obtain more model data of hexagonal aperture lens, during the fabrication of array lens, array elements with different types of distance are assembled on the same substrate and arranged at different distance within the range of *3.5 mm* × *3.5 mm*, as shown in Fig 4. The distances between the two adjacent lens elements were *1.25 mm*, *1 mm*, *0.875 mm* and *0.5 mm*, respectively. It can be seen that the smaller the distance between two adjacent lens elements, the more information will be obtained, which is also onducive to improving the experimental accuracy. Therefore, this paper selected the distance of lens array as *0.5 mm*, the refractive index of lens material as *1.49*, the focal length of each lens element as *6 mm* and the radius of curvature as *2.94 mm* [17]–[21].

Digital image processing technology was used to identify and calculate the spot images collected by the CCD. To ensure that the diffraction ring does not affect the measurement results, the spots cannot overlap.

The light source is diffracted by an imaging lens unit, and the first-order diffraction angle is

$$\varphi = \frac{1.22\lambda}{D} \tag{9}$$

where D is the diameter of the lens unit aperture and λ is the wavelength of the light source. In this paper, $D = 0.5\ mm$, the wavelength of the He–Ne laser is *632.8 nm*, thus the first-order diffraction angle is

$$\varphi = \frac{1.22\lambda}{D} = \frac{1.22 \times 632.8 \times 10^{-6}}{0.5} \approx 0.00154\text{rad} \tag{10}$$

The diameter of the first-order diffraction ring on the CCD is

$$d = \varphi \times b = \frac{1.22\lambda}{D} \times b \tag{11}$$

where b is the maximum distance from the array lens to the CCD, and we can obtain $d = 0.00154 \times 6.25 \approx 0.0096\ mm$.

For digital imaging, the distance between two adjacent spots on the CCD was approximately *0.5 mm*, and the diameter of the first-order diffraction ring was much smaller than the distance between adjacent spots. Therefore, the effect of diffraction on the measurement results can be ignored.

In addition, we can ensure that the spot does not overlap on the CCD by controlling the distance between the CCD and array lens, lens focal length, array distance, and other parameters.

V. PROCESSING METHOD OF MULTI-SPOT IMAGE CENTROID

In this study, the measurement of the beam incidence angle is mainly divided into two steps. First, according to the spot array image detected by CCD, the spot centroid position of each sub-aperture was calculated, and then the distance between adjacent spots can be obtained. Second, based on the distance between adjacent spots, the corresponding data were processed using the beam incidence angle measurement formula.

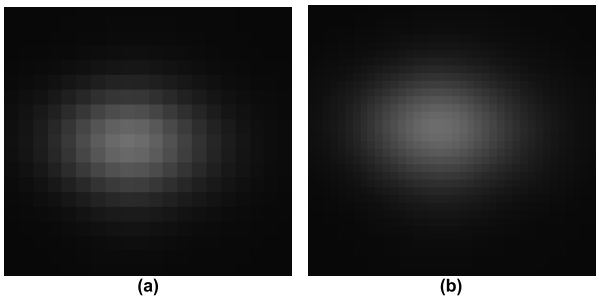

FIGURE 5. The spot image before and after interpolation: (a) the spot image before interpolation, (b) the spot image after interpolation.

A. FOR THE PROCESSING OF THE SPOTS ARRAY IMAGE

To improve the accuracy of spot distance detection, the spot array image is preprocessed by filtering to eliminate stray light and random noise, while the features of the spot signal are kept as far as possible, and the image is processed by binarization.

Then, the detection window was segmented by the iterative threshold method, and the minimum grayscale value G_{min} and the maximum grayscale value G_{max} after denoising were calculated. Setting the initial threshold as $T_k = (G_{min} + G_{max})/2$, dividing the image into foreground and background images according to the threshold T_k, and calculating the average gray value G_0 and G_1 of these two parts of the image; then, the new threshold is $T_{k+1} = (G_0 + G_1)/2$.

If $T_k = T_{k+1}$, the iteration ends. Otherwise, T_{k+1} replaces T_k and iterates again until $T_k = T_{k+1}$. Here T_k is the global threshold T, and the detection window of the spot array image is obtained through global threshold segmentation.

After the detection window was obtained, the pixel was subdivided using the interpolation method in image processing. This is equivalent to increasing the available points per unit area, reducing the pixel size, improving the image resolution of the CCD and reducing the image dispersion; so that the detected image is closer to the original image. The linear interpolation method can achieve satisfactory results for low-power interpolation and consumes less time; therefore, it is selected to process the spot image. In a certain detection window, the image is first interpolated linearly, the centroid of the spot is then calculated, and the distance between adjacent spots is obtained.

Fig. 5 shows the spot image before and after interpolation in one of the detection windows. The size of the original image was 17pixel × 18pixel, and the size of the interpolated image was 34pixel × 37pixel.

B. FOR THE OPTIMAL ESTIMATE OF THE DISTANCE BETWEEN MULITIPLE SPOTS

After preprocessing the spot image, the exact location of the spot centroid can be determined using the first-moment spot centroid detection method [22]. The equation for calculating the centroid of the first subaperture spot is given by (12). Where $\bar{x}_i$ and $\bar{y}_i$ are the centroid coordinates of the spot in the i_{th} subaperture, I_{nm} is the pixel intensity value at location (n, m), x_{nm} and y_{nm} are the pixel coordinates at the location (n, m), respectively, and the size of the sub-aperture is N pixel × M pixel. According to the centroid coordinates, the distance between the i_{th} and $(i\text{-}1)_{th}$ spots can be obtained using (13).

$$\begin{cases} \bar{x}_i = \dfrac{\sum_{m=1}^{M}\sum_{n=1}^{n} x_{nm} I_{nm}}{\sum_{m=1}^{M}\sum_{n=1}^{n} I_{nm}} \\ \bar{y}_i = \dfrac{\sum_{m=1}^{M}\sum_{n=1}^{n} y_{nm} I_{nm}}{\sum_{m=1}^{M}\sum_{n=1}^{n} I_{nm}} \end{cases} \tag{12}$$

$$h = \sqrt{(\bar{x}_i - \bar{x}_{i-1})^2 + (\bar{y}_i - \bar{y}_{i-1})^2} \tag{13}$$

By processing the data of the adjacent spot distance h_i, the average spot distance $\bar{h}$ and residual error v_i of the measured spot distance can be calculated as

$$\bar{h} = \frac{\sum_{i=1}^{n} h_i}{n} \tag{14}$$

$$v_i = h_i - \bar{h} \tag{15}$$

According to the algebra of residual errors and the test rules, and using the symmetry of random errors, if (16) is correct, the above calculation can be judged to be correct.

$$\left|\sum_{i=1}^{n} v_i\right| \approx 0 \tag{16}$$

Otherwise, the above calculations and tests should be carried out again.

The number of positive and negative residual errors can be determined using the residual error observation method. If the number of positive and negative errors is almost equal, and the distribution of the errors is random, it can be judged that there is no systematic error in this group of measurement data. The standard deviation of the distance between adjacent light spots can then be obtained using the Bessel function:

$$\sigma = \sqrt{\sum_{i=1}^{n} v_i^2/(n-1)} \tag{17}$$

According to the 3σ criterion:

$$|v_i| > 3\sigma \tag{18}$$

The measurement value was considered to contain gross errors that should be eliminated. The spot distance values were iterated until the gross error was completely eliminated. The other values were the optimal spot-distance measurement values without any gross errors.

VI. EXPERIMENTAL RESULTS AND ANALYSIS

A. EXPERIMENTAL PLATFORM

As shown in Fig. 6, the entire system is composed of two parts: a measurement unit including a laser source, lens array arranged by a pyramid taper and CCD camera. The second part is a verification unit composed of two autocollimators

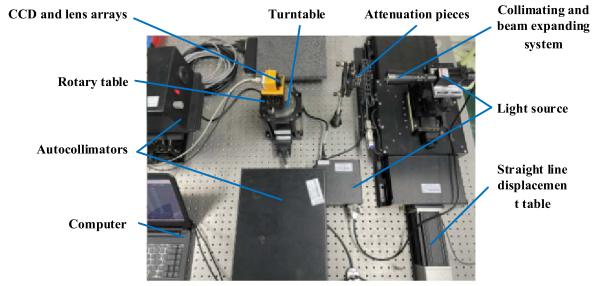

FIGURE 6. Measurement experiment platform.

and a turntable. The lens arrays and CCD were integrated in a frame, and fixed to the turntable. Different angles of the frame relative to the coordinate axes X, Y, and Z can be obtained. If we adjust the turntable or screw, the spot array can be obtained from the CCD. When the values of the spot distance and coordinates are substituted into (2) and (5), respectively, the spatial angle of the laser source relative to the frame can be obtained.

In the experiment, the resolution ratio and the pixel size of CCD are 2048pixel $\times$ 2048pixel and $6.5\mu m \times 6.5\mu m$, the size of aperture of the sub-lens is $1mm \times 1mm$ and the focal length is 30 mm. Two autocollimators were arranged orthomorphically in the experimental system, and the measurement accuracy was less than $0.1''$ for each of them. Autocollimator 1 obtains the angles of the frame around the X and Y axes depending on laser beam 1 reflected by mirror 1 attached to the frame, and autocollimator 2 obtains the angle of the frame around the Z axes using the same theory.

B. CALIBRATION OF THE ANGLE α

The motion controller controlled the turntable to rotate the angle clockwise, and the exact value of the angle increment, $\Delta\beta$, was read on the autocollimator. Simultaneously, the spot image was intercepted, and the distance h between adjacent spots in the *X-direction* was obtained through image processing.

Through cyclic measurements, 23 groups of data were collected accumulatively, and angle increments $\Delta\beta i(1 \leq i \leq 23)$ were obtained. Under the influence of errors such as rotary table accuracy, CCD pixel size, and image processing, the angle increment was set relatively large in the experiment in this study to reflect the changing trend of the spot distance. The corresponding 23 groups of adjacent spot distance values $h_i(1 \leqslant i \leqslant 23)$ were obtained, as listed in Table 1, which the 7th group spots array is shown in Fig. 7.

Because the distance between adjacent lens elements of the lens array is 0.5mm, that is, $l = 0.5$mm.

In this paper, the Matlab software was used to perform data fitting for the 23 groups of data. To complete the estimation and solution of the nonlinear complex model in (8), the least-square method was used for fitting and the optimal solution was found. Fig. 8 shows the data-fitting diagram of the distance between adjacent spots.

The deviation of angle α between the lens array and CCD is a systematic error. The system error compensation is

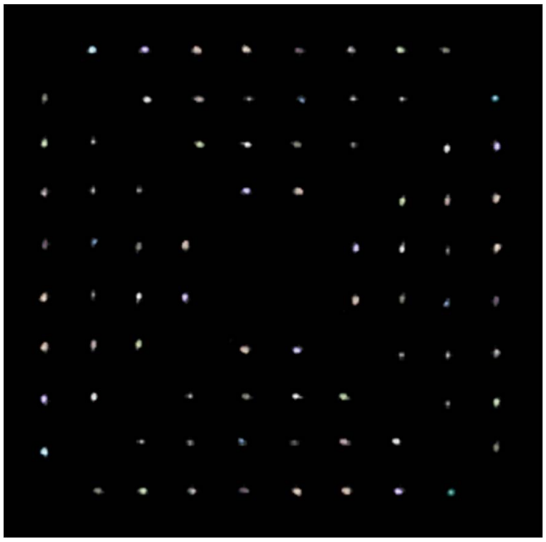

FIGURE 7. The 7th group spots array.

TABLE 1. The measured results of $\Delta\beta$ and h.

Group	Δβ(″)	h(mm)	Group	Δβ(″)	h(mm)
1	90.56	0.47059	13	1116.22	0.46946
2	172.38	0.47041	14	1202.42	0.46924
3	250.95	0.47034	15	1298.75	0.46906
4	370.93	0.47021	16	1394.92	0.46897
5	430.44	0.47012	17	1506.51	0.46888
6	560.07	0.47010	18	1591.23	0.46885
7	621.27	0.47005	19	1715.49	0.46875
8	709.03	0.47000	20	1902.03	0.46860
9	798.08	0.46989	21	1997.47	0.46843
10	867.35	0.46976	22	2108.96	0.46825
11	943.59	0.46966	23	2210.34	0.46816
12	1035.85	0.46951			

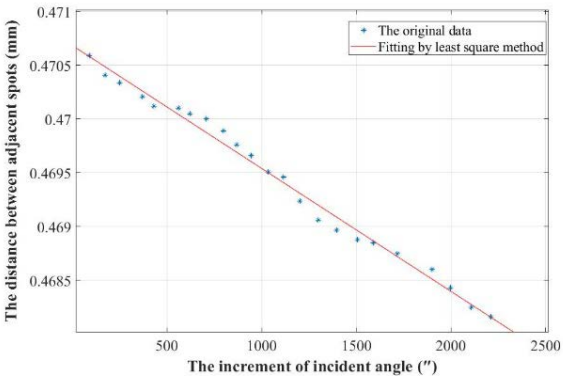

FIGURE 8. The data fitting diagram of the distance between adjacent spots.

performed by the angle calibration of α; that is, the compensation information of the α value is obtained by the increment of the incident angle with relative truth value characteristics. Least squares fitting with the first-order function was used to obtain the best adjustment compensation. The relationship between the distance h between adjacent spots and the incident angle β is

$$h = 0.4707 - 0.00411\beta \tag{19}$$

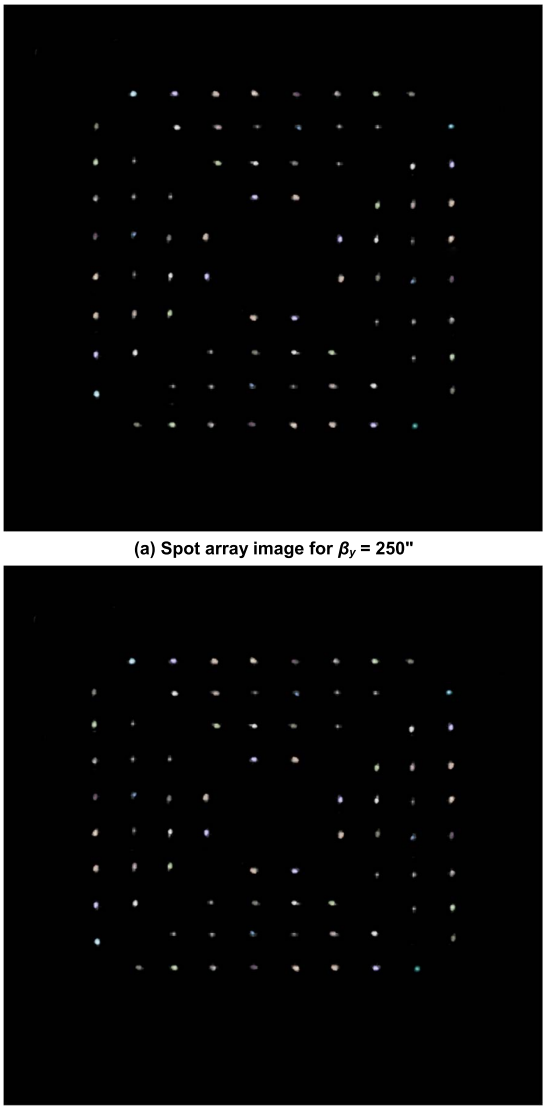

(a) Spot array image for β_y = 250"

(b) Spot array image for β_y = 500"

FIGURE 9. Image of spot array with β_y variation.

Namely, the equation of the incident angle after compensation is:

$$\beta = 412291.97 - 875912.41h \tag{20}$$

where, the unit of incident angle β is second, and the unit of distance h between adjacent spots is millimeter.

C. DATA OF EXPERIMENTAL PROCESS

After calibration and compensation for α, when the incident beam only has a tilt angle in the *Y-direction*, the corresponding angle spot image is shown in Fig. 9.

D. ANALYSIS OF EXPERIMENTAL RESULT

The experimental results showed that the angle β_y of the incident beam in the *Y-direction* can be calculated from the spot distance of lens arrays 2 and 4 along the *Y-direction*. The result when the incident beam had a tilt angle only in the Y direction is shown in Fig. 9, where the distance of

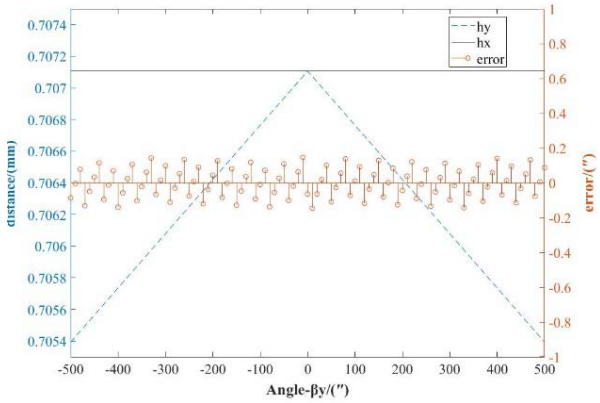

FIGURE 10. Measurement results in the Y direction.

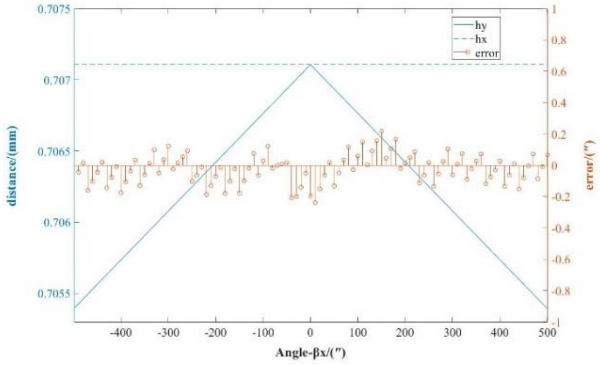

FIGURE 11. Measurement results in the *X* direction.

h_x or h_y is the mean of the distance of adjacent points in each row or column, respectively. As shown in Fig. 10, the distance between adjacent spot arrays in the X direction was consistent with that expected, while the distance in the Y direction decreased with an increase in the distance between the angle β_y and the equilibrium position $\beta_y = 0$. The RMS error between the autocollimator and measured angle was $0.085''$.

Similarly, when the incident beam had a slant angle only in the *X-direction*, the relationship between the average distance of the spot array obtained using lens 1 and 3 and the slant angle value β_x was obtained, as shown in Fig. 11. The distance of the spot array in the Y direction, h_y, remained constant, whereas the distance in the X direction, h_x, decreased as the deviation from the equilibrium position $\beta_x = 0$ increased. The RMS of the angle error was $0.094''$. As shown in Fig. 1(a), a similar phenomenon occurs when the angle of the incident beam is slanted and tilted in either the *X-* or *Y-direction* owing to the symmetry of the measured structure.

When the incident beam is twisted along the *Z-axis*, several groups of feature points are selected on the spot formed by lens arrays 1 to 4 to calculate the change in the centroid $(\Delta x, \Delta y)$. The average torsion angle γ is obtained from (5), as shown in Fig. 12. In the *X-* and *Y-directions*, the distance between the spot arrays remained unchanged, and the RMS of the torsion angle γ was $0.092''$.

The relationship between the centroid variations Δx and Δy and torsion angle γ is shown in Fig. 13. With the change

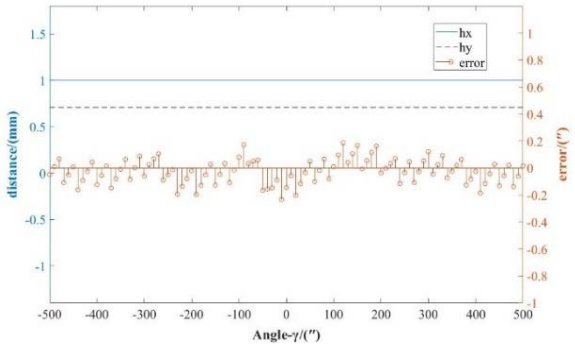

FIGURE 12. Measurement results in the *Z* direction.

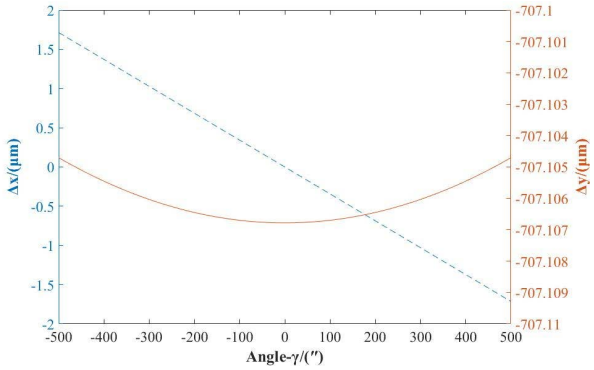

FIGURE 13. Curve of centroid variation with Z direction torsion angle.

in the spot centroid variation Δx in the X direction, if the variation was positive, the beam rotated clockwise; otherwise, it rotated counter-clockwise. The small variation in the *Y-direction* Δy increased with an increase in the torsion angle. Therefore, when rotating clockwise, the measurement result was negative; in contrast, the result was positive. In addition, the trajectory of the feature points is approximated as a circle.

The three main sources of error affect the measurement accuracy of the system. The first error source is the error in the installation angle α of the microlens array relative to the CCD sensor plane. This is a systematic error. The method to eliminate this error is given in this paper in Section B Part VI, that is, the calibration of angle α. The second source of error is the uneven fabrication of the microlens array. The processing errors of different lens elements in the microlens array lead to a change in the focal length of the lens, which affects the spot imaging quality. Manufacturing error can be solved by calibration. The measurement system designed in this study adopts relative measurement, which can correct manufacturing error and system error through calibration. The third error source is the solution of the spot centroid. The calculation accuracy of the spot centroid directly affected the measurement accuracy of the system developed in this study.

Taking the angle deviation in the *X-direction* as an example, repeatability and stability tests were conducted at three different positions within $\pm 500''$, as shown in Fig. 14. At position $X = -250''$, the RMS value of the stability error was $0.0156''$. At position $X = 0''$, the RMS value of the

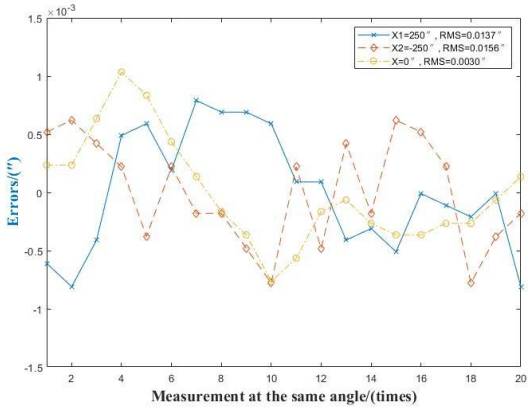

FIGURE 14. Stability error test in 3 different positions of X direction.

stability error was $0.0030''$. At position $X = +250''$, the RMS value of the stability error was $0.0137''$.

VII. CONCLUSION

In summary, this study argues that the inclination angle β of the incident beam in the X and Y directions and the torsion angle γ in the Z direction can be calculated from the spot distance of the pyramid lens array. The inclination component βx of the incident beam in the X direction can be obtained from the spot distance of the spot array formed by lens arrays 1 and 3, the inclination component β_y in the Y direction can be obtained by the spot distance of the spot array formed by lens arrays 2 and 4, the torsion angle γ in the Z direction can be obtained by four feature points of the lens array, and RMS $\leq 0.1''$. Compared with the autocollimator angle measuring method, which has the highest accuracy in measuring small-angle current, this method has the advantage of a small volume and is easy to carry. Therefore, after structural transformation and optimization, the measurement principle can be applied for the detection of smile acceleration. With the miniaturization of measurement angle, the influence of the measurement error on the results is also increasing, and future research should be devoted to improving the measurement accuracy based on this measurement method. The accuracy of this method can be improved from the following two aspects: spot centroid extraction and lens array model optimization.

ACKNOWLEDGMENT

The lens array for the experiment was fabricated by Allen Yi's group from The Ohio State University.

REFERENCES

[1] A. A. B. Raj, A. J. V. Selvi, K. D. Durai, and R. S. Singaravelu, "Intensity feedback-based beam wandering mitigation in free-space optical communication using neural control technique," *EURASIP J. Wireless Commun. Netw.*, vol. 2014, no. 1, pp. 1–18, Dec. 2014.

[2] S. Bai, J. Wang, J. Qiang, L. Zhang, and J. Wang, "Predictive filtering-based fast reacquisition approach for space-borne acquisition, tracking, and pointing systems," *Opt. Exp.*, vol. 22, no. 22, pp. 26462–26475, 2014.

[3] P.-H. Hu, C.-W. Yu, K.-C. Fan, X.-M. Dang, and R.-J. Li, "Error averaging effect in parallel mechanism coordinate measuring machine," *Appl. Sci.*, vol. 6, no. 12, p. 383, Nov. 2016.

[4] M. L. D. Scherff, J. Nutter, P. Fuss-Kailuweit, J. Suthues, and T. Brammer, "Spectral mismatch and solar simulator quality factor in advanced LED solar simulators," *Jpn. J. Appl. Phys.*, vol. 56, no. 8S2, Aug. 2017, Art. no. 08MB24.
[5] S. Tang, Z. Wang, J. Gao, and L. Zhong, "Influence of tilt on collinear calibration of a laser interferometer," *Appl. Opt.*, vol. 52, no. 4, pp. 46–51, 2013.
[6] Y. Saito, W. Gao, and S. Kiyono, "A micro-angle sensor based on laser autocollimation," in *Proc. Optomechatronic Syst. Control*, Dec. 2005, Art. no. 60520Q.
[7] M. D. Lian, W. F. Jin, and B. F. Ju, "2D micro-angle sensor based on laser autocollimation," *J. Mech. Electr. Eng.*, vol. 27, no. 12, pp. 23–26, 2010.
[8] H. L. Hsieh and S. W. Pan, "Development of a grating-based interferometer for six-degree-of-freedom displacement and angle measurements," *Opt. Exp.*, vol. 23, no. 3, pp. 2451–2465, 2015.
[9] Q. B. Feng, Z. Bin, C. Cunxing, K. Cuifang, Z. Yusheng, and Y. Fenglin, "Development of a simple system for simultaneously measuring 6DOF geometric motion errors of a linear guide," *Opt. Exp.*, vol. 21, no. 22, pp. 25805–25819, Nov. 2013.
[10] A. Sabatyan and S. A. Hoseini, "Fresnel biprism as a 1D refractive axicon," *Optik*, vol. 124, no. 21, pp. 5046–5048, Nov. 2013.
[11] E. Zhang, B. Chen, H. Zheng, X. Teng, and L. Yan, "Note: Comparison experimental results of the laser heterodyne interferometer for angle measurement based on the Faraday effect," *Rev. Sci. Instrum.*, vol. 89, no. 4, Apr. 2018, Art. no. 046104.
[12] Y. Wu, H. Cheng, and Y. Wen, "High-precision rotation angle measurement method based on a lensless digital holographic microscope," *Appl. Opt.*, vol. 57, no. 1, p. 112, 2018.
[13] J. Yuan, P. Dai, D. Liang, S. Zhou, S. Xiao, and X. Liang, "Grid deformation real-time measurement system of ion thruster based on videometrics," *Appl. Sci.*, vol. 9, no. 9, p. 1759, Apr. 2019.
[14] I. Konyakhin, A. M. Sakhariyanova, and A. Smekhov, "Investigation vignetting beams in optoelectronic autocollimation angle measurement system," *Opt. Metrol.*, vol. 9526, 2015, Art. no. 95260H.
[15] Y.-L. Chen, Y. Shimizu, J. Tamada, K. Nakamura, H. Matsukuma, X. Chen, and W. Gao, "Laser autocollimation based on an optical frequency comb for absolute angular position measurement," *Precis. Eng.*, vol. 54, pp. 284–293, Oct. 2018.
[16] S. K. Sarkar, A. Basuray, and K. Sengupta, "A compound interferometer for angle measurement," *Opt. Commun.*, vol. 89, nos. 2–4, pp. 153–158, May 1992.
[17] S. A. Shaikh and A. M. Tonello, "Radio source localization in multipath channels using EM lens assisted massive antennas arrays," *IEEE Access*, vol. 7, pp. 9001–9012, 2019.
[18] Y.-K. Fuh and Z.-H. Lai, "A fast processing route of aspheric polydimethylsiloxane lenses array (APLA) and optical characterization for smartphone microscopy," *Opt. Commun.*, vol. 385, pp. 160–166, Feb. 2017.
[19] X. Chang, K. Xu, D. Xie, S. Luo, X. Shu, H. Ding, K. Zheng, and B. Li, "Microforging technique for fabrication of spherical lens array mold," *Int. J. Adv. Manuf. Technol.*, vol. 96, nos. 9–12, pp. 3843–3850, Jun. 2018.
[20] S. Coppola, V. Pagliarulo, V. Vespini, G. Nasti, F. Olivieri, S. Grilli, and P. Ferraro, "Direct fabrication of polymer micro-lens array," *Proc. SPIE*, vol. 10329, Jul. 2017, Art. no. 103294Q.
[21] K. H. Liu, M. F. Chen, C. T. Pan, M. Y. Chang, and W. Y. Huang, "Fabrication of various dimensions of high fill-factor micro-lens arrays for OLED package," *Sens. Actuators A, Phys.*, vol. 159, no. 1, pp. 126–134, Apr. 2010.
[22] Y. Y. Zhang, X. L. Hao, and J. W. Chen, "First moment spot centroid detection with a threshold to compute the centroid," *Opt. Technique*, vol. 41, no. 1, pp. 59–63, 2015.
[23] F. M. Zhang and L. Song, "A new MATLAB de-noising algorithm for signal extraction," *Int. J. Plant Eng. Manage.*, vol. 12, no. 1, pp. 18–23, 2007.
[24] W. Zhengang, Z. Zhoumo, L. Xingqiang, W. Xiangyu, and F. Luhua, "Non-contact *in-situ* dihedral angle measuring approach base on rotary ray-scanning mechanism," *Chin. J. Lasers*, vol. 43, no. 5, 2016, Art. no. 0508001.
[25] H. Yu, Q. Wan, X. Lu, C. Zhao, and Y. Du, "A robust sub-pixel subdivision algorithm for image-type angular displacement measurement," *Opt. Laser. Eng.*, vol. 100, pp. 234–238, Jan. 2018.
[26] J. Rodriguez-Maldonado, "Estimation of angular velocity and acceleration with Kalman filter, based on position measurement only," *Measurement*, vol. 145, pp. 130–136, Oct. 2019.
[27] M. Dobosz, M. Jankowski, and J. Mruk, "Application of interference sensor of angular micro-displacement in measurements of machine rotational errors," *Precis. Eng.*, vol. 60, pp. 12–20, Nov. 2019.
[28] H. Yu, X. Jia, Q. Wan, C. Zhao, and Y. Sun, "High-resolution angular measurement arithmetic based on pixel interpolations," *Measurement*, vol. 149, Jan. 2020, Art. no. 106948.
[29] W. Congjun, Y. Changxiang, and L. Wei, "Analysis of optical aberration impact on acquisition performance," *Chin. J. Lasers*, vol. 40, no. 10, 2013, Art. no. 1005004.

CUNLIANG CAI received the B.S. and M.Sc. degrees in instrument science and technology from the Changchun University of Science and Technology, China, in 2012 and 2015, respectively, where he is currently pursuing the Ph.D. degree with the School of Opto-Electronic Engineering.

He is also an Experimentalist with the School of Opto-Electronic Engineering, Changchun University of Science and Technology. His current research interests include optical measurement, photoelectric detection technology, instrument accuracy analysis, overall design, simulation of precision instruments, and automatic electric control.

YUFENG YAN received the Ph.D. degree in instrument science and technology from the Changchun University of Science and Technology, China, in 2010.

He is currently a Professor with the School of Opto-Electronic Engineering, Changchun University of Science and Technology. His current research interests include optical mechanical system design, photoelectric detection technology, instrument accuracy analysis, and optical measurement.

LEI ZHANG is currently ranked as an Engineer. His current research interest includes measurement technology.

MINGXIN DU received the degree in instrumentation science and technology from the Changchun University of Science and Technology, where he is currently pursuing the master's degree. His current research interests include optical-mechanical system design, roll angle measurement techniques, photoelectric detection technology, and error analysis.

XIN YU received the M.Sc. degree from the Changchun University of Science and Technology, China, in 2014, and the Ph.D. degree from the University of Electronic Science and Technology of China, in 2018.

He is currently a Lecturer with the School of Opto-Electronic Engineering, Changchun University of Science and Technology. His current research interests include aberration detection and correction, and precision instrument design.